Supplemental Material

Deficient Circumferential Growth is the Primary Determinant of Aortic Obstruction Attributable to Partial Elastin Deficiency

Yang Jiao, Guangxin Li, Arina Korneva, Alexander W. Caulk, Lingfeng Qin, Matthew R. Bersi, Qingle Li, Wei Li, Robert P. Mecham, Jay D. Humphrey, and George Tellides

Appendix I: Area Conserving Medial Remodeling

The observation that inward wall remodeling in WS tends to preserve the cross-sectional area of the media invites a simple mathematical study. Let the normal luminal radius be denoted by a and the normal medial thickness be denoted by b. Medial cross-sectional area A is thus given by $A = \pi b(2a + b)$. If we let a perturbed luminal radius be given by αa and the associated perturbed medial thickness be given by βb, where α and β simply denote fold-changes (e.g., $\alpha = 0.9$ if the inner radius decreases by 10% or $\alpha = 1.1$ if the inner radius increases by 10%) and if we assume that the perturbed (new) cross-sectional area equals the normal area, then $A = \pi b(2a + b) = \pi\beta b(2\alpha a + \beta b)$, which admits a solution for the change in medial thickness that is required to maintain medial area constant despite a change in luminal radius, namely

$$\beta = -\alpha\left(\frac{a}{b}\right) \pm \sqrt{\alpha^2\left(\frac{a}{b}\right)^2 + 2\left(\frac{a}{b}\right) + 1}. \quad (1)$$

Consequences of this constraint are seen in Supplemental Fig. VII.

Appendix II: Further Questions Generated by New Hypothesis

Our findings generate several unanswered questions that warrant investigation in future studies. First, is whether the mechanisms causing clinical lesions differ according to elastin content and disease severity? Although the aortopathy of WS reflects *ELN* haploinsufficiency, the expression of elastin or the effects of elastin deficiency may be modulated by other genes and thus vary according to genetic background. Additionally, local loss of elastin (cf. ascending aorta discussion below) or local distortion of elastin architecture (e.g., at branch points) may unmask excessive SMC proliferation. For example, mild-to-moderate diffuse lesions resulting from decreased circumferential growth may progress to severe disease at focal sites if an additional pathological process, including SMC hyperplasia, is superimposed. Indeed, it appears that medial expansion, likely associated with increased numbers of SMCs, contributes to severe lesions of WS patients requiring invasive intervention early in life [1]. Differences in elastin expression may explain why in vitro conditions with minimal ECM elaborated by cultured cells enables their increased proliferation [2,3], including cultured SMCs from the same WS subject characterized in the present report [4]. Similarly, lower elastin expression may also explain the discordant observations in heterozygous $Eln^{+/-}$ mice of SMC de-differentiation and loss of contractile molecules in vitro [3], but intact vasoconstrictor responses by aortic rings in situ [5]. Quantifying elastin transcripts, even in non-vascular tissue or cultured cells, may detect gene interaction effects on synthesis by the remaining *ELN* allele [2], however protein measurement within vessel wall lesions is necessary to evaluate for local loss of elastin, e.g., damage by mechanical fatigue or proteolytic degradation. Assessment of elastin content by histo-morphometric techniques, as in our study, provides spatially restricted results, but represents relative values and requires batch processing to enable comparisons among multiple specimens. In contrast, biochemical analysis of elastin content as pmol desmosine per mg protein is a quantitative technique [6], but prone to contamination by tissues other than the tunica media. Elucidation of mechanisms responsible for the full spectrum of aortic obstruction in WS will require measurements of mural thickness, area, and volume, in addition to vessel diameter, length, and distensibility, in severe as well as mild-to-moderate cases. This is possible only by advanced imaging techniques as the latter subjects are unlikely to undergo surgery or postmortem examination.

Second, is why the ascending aorta preferentially manifests elastin-related abnormalities and disease? Within the same WS aortas, there is far less, if any, elastin dysplasia in descending compared with ascending segments [7]. Indeed, the descending aorta was examined to document the increased number of elastic laminae as those of the ascending aorta were too irregular and fragmented to count [8]. Reasons for the marked predilection of the proximal aorta to elastin arteriopathy are unknown, but differences in wall structure, mechanics, and cell lineage should be considered. The ascending portion of the aorta normally has the highest elastin content and it alone is subject to biaxial loading (distension and extension) upon each cardiac cycle [9]. Sites of highest synthesis may be most affected by gene haplo-insufficiency, and greater mechanical stresses may further disrupt abnormal elastic fibers. We find a 43% greater loss of elastin in the ascending than descending aorta of hBAC-mNULL mice consistent with the two-fold greater elastin deficiency in the ascending compared to abdominal aorta of this strain [6]. We also find an 82% lower elastin content in the ascending aorta versus a minimal 2% difference in the descending aorta of our WS subject. Clinical corroboration for our premise is that elastin architecture appears more fragmented within a focal stenotic lesion than in the remaining ascending aorta of the same WS patient [2]. Furthermore, the embryological origin of SMCs in the ascending aorta and aortic arch is the neural crest, which is not the case for the remaining aorta [10]. Analysis of clinical lesions for markers indicative of neural crest origin may be informative, as may conditional deletion of *Eln* in SMCs of different origins in murine genetic models. Injury models of the mouse aorta are unlikely to be useful as a model of obstructive medial expansion due to SMC loss and/or migration into the intima.

Third, is how elastin deficiency retards circumferential growth of the aorta? Although the molecular mechanisms of this process remain to be determined, we hypothesize that altered mechanosensing by medial SMCs plays a central role. Abnormalities of elastin architecture and associated changes in collagen expression may alter mechanotransduction from the ECM to membrane integrin receptors. Specifically, loss of stress shielding by the ECM and changes in microfibrillar connections between SMCs and elastic laminae may result in mis-sensing of hemodynamic forces [11]. Lower wall stresses in elastin-deficient aortas may further contribute to disordered vessel growth. Strikingly, reduced *Itgb3* gene dosage in *Eln*$^{-/-}$ null mice led to larger diameter ascending aortas in addition to reducing SMC proliferation and luminal obstruction [12]. Our preliminary findings regarding expression differences in particular collagens and collagen receptors offer a basis for loss-of-function approaches to test this hypothesis.

References

1. Rein AJ, Preminger TJ, Perry SB, Lock JE, Sanders SP. Generalized arteriopathy in Williams syndrome: an intravascular ultrasound study. *J Am Coll Cardiol*. 1993;21:1727-30.
2. Urbán Z, Riazi S, Seidl TL, Katahira J, Smoot LB, Chitayat D, Boyd CD, Hinek A. Connection between elastin haploinsufficiency and increased cell proliferation in patients with supravalvular aortic stenosis and Williams-Beuren syndrome. *Am J Hum Genet*. 2002;71:30-44.
3. Karnik SK, Brooke BS, Bayes-Genis A, Sorensen L, Wythe JD, Schwartz RS, Keating MT, Li DY. A critical role for elastin signaling in vascular morphogenesis and disease. *Development*. 2003;130:411-23.
4. Li W, Li Q, Qin L, Ali R, Qyang Y, Tassabehji M, Pober BR, Sessa WC, Giordano FJ, Tellides G. Rapamycin inhibits smooth muscle cell proliferation and obstructive arteriopathy attributable to elastin deficiency. *Arterioscler Thromb Vasc Biol*. 2013;33:1028-35.
5. Faury G, Pezet M, Knutsen RH, Boyle WA, Heximer SP, McLean SE, Minkes RK, Blumer KJ, Kovacs A, Kelly DP, Li DY, Starcher B, Mecham RP. Developmental adaptation of the mouse cardiovascular system to elastin haploinsufficiency. *J Clin Invest*. 2003;112:1419-28.
6. Hirano E, Knutsen RH, Sugitani H, Ciliberto CH, Mecham RP. Functional rescue of elastin insufficiency in mice by the human elastin gene: implications for mouse models of human disease. *Circ Res*. 2007;101:523-31.
7. van Son JA, Edwards WD, Danielson GK. Pathology of coronary arteries, myocardium, and great arteries in supravalvular aortic stenosis. Report of five cases with implications for surgical treatment. *J Thorac Cardiovasc Surg*. 1994;108:21-8.
8. Li DY, Faury G, Taylor DG, Davis EC, Boyle WA, Mecham RP, Stenzel P, Boak B, Keating MT. Novel arterial pathology in mice and humans hemizygous for elastin. *J Clin Invest*. 1998;102:1783-7.
9. Roccabianca S, Figueroa CA, Tellides G, Humphrey JD. Quantification of regional differences in aortic stiffness in the aging human. *J Mech Behav Biomed Mater*. 2014;29:618-34.
10. Majesky MW. Developmental basis of vascular smooth muscle diversity. *Arterioscler Thromb Vasc Biol*. 2007;27:1248-58.
11. Humphrey JD, Milewicz DM, Tellides G, Schwartz MA. Cell biology. Dysfunctional mechanosensing in aneurysms. *Science*. 2014;344:477-9.
12. Misra A, Sheikh AQ, Kumar A, Luo J, Zhang J, Hinton RB, Smoot L, Kaplan P, Urban Z, Qyang Y, Tellides G, Greif DM. Integrin β3 inhibition is a therapeutic strategy for supravalvular aortic stenosis. *J Exp Med*. 2016;213:451-63.

Table I: Summary of the Analytical Techniques to Assess the Murine Thoracic Aorta

Approach	Description of approach	Measurement (arterial segment)
In Vivo	Antemortem assessment using ultrasound	Internal diameter: end-systolic/end-diastolic (ascending) Distension (ascending)
	Antemortem assessment by tail-cuff	Blood pressure: systolic/diastolic/mean (peripheral artery)
In Situ	Postmortem examination after thoracotomy	Width/external diameter (ascending, arch, descending) Length (ascending, arch, descending)
Ex Vivo	Postmortem examination after excision of aorta	Mass (entire thoracic aorta)
	Biomechanical phenotyping (biaxial testing)	Dimension: diameter, wall thickness (ascending, descending) Circumferential and axial stretch (ascending, descending) Circumferential and axial stress (ascending, descending) Circumferential and axial stiffness (ascending, descending) Distensibility (ascending, descending) Elastically stored energy (ascending, descending)
Histology	H&E	Number of medial cells (ascending)
	EVG	Media thickness and area (ascending, descending) Adventitia thickness (ascending) Lumen area (ascending)
	Elastin	Elastin content of media (ascending, descending)
	Sirius red	Collagen content of media (ascending, descending) Collagen content of adventitia (ascending)
Immunohisto-chemistry	BrdU antibody	Proliferation of medial cells (ascending and descending)
	SMA antibody	SMA protein expression (ascending)
qRT-PCR	RNA sequence-specific primers and probes	*Acta2*, *Myh11*, *Myl6*, *Col1a1*, *Col3a1*, *Col8a1*, *Col11a1*, *Itga11*, *Itgb1*, *Eln*, *ELN*, *Gapdh*, *Actb*, and *Hprt* (entire thoracic aorta)

A caveat to the methodology is that measurements of the aorta differ in vivo compared to postmortem techniques in situ (reflecting a loss of hemodynamic forces), ex vivo (additionally reflecting a loss of tethering to arterial branches and surrounding tissue), and by histology (also subject to formalin fixation artifact). For example, external diameter measurements of the ascending aorta from histological sections were on average 16.2% less than in situ gross images. In turn, in situ external diameter differed by only 1.6% from end-diastolic internal diameters and by 17.9% from end-systolic internal diameters as measured by ultrasound in vivo. In situ and ex vivo measurements were applied to the entire thoracic aorta, whereas in vivo ultrasound examination was only applicable to the ascending aorta. Another methodological limitation is that determining the number of medial cells by counting nuclei in transverse sections assumes a similar orientation of SMCs among genotypes.

Table II: Summary of Biomechanical Data in Numerical Form

	ATA			DTA		
	hBAC-mWT (n=5)	**WT (n=5)**	**hBAC-mNULL (n=7)**	**hBAC-mWT (n=5)**	**WT (n=5)**	**hBAC-mNULL (n=6)**
Unloaded dimensions						
Inner Diameter (μm)	979 +/- 24	871 +/- 33	594 +/- 19**	635 +/- 17	680 +/- 13	420 +/- 16**
Wall Thickness (μm)	108 +/- 4.0	112 +/- 1.8	153 +/- 5.2**	106 +/- 6.2	111 +/- 4.5	149 +/- 3.0**
Outer Diameter (μm)	1194 +/- 26	1094 +/- 30	901 +/- 24**	848 +/- 8*	902 +/- 8	718 +/- 17**
Loaded dimensions (Psys=129mmHg)						
Inner Diameter (μm)	1893 +/- 45	1739 +/- 64	1041 +/- 44 **	1402 +/- 29	1386 +/- 35	923 +/- 30**
Wall Thickness (μm)	34 +/- 1.9	35 +/- 0.9	70 +/- 2.5**	36 +/- 1.3	38 +/- 1.5	57 +/- 1.3**
Outer Diameter (μm)	1960 +/- 46	1809 +/- 63	1181 +/- 42 **	1475 +/- 28	1463 +/- 33	1038 +/- 31**
Ratio Inner Radius to Thickness	28 +/- 1.5	25 +/- 1.2	8 +/- 0.5**	19 +/- 0.9	18 +/- 1.0	8 +/- 0.3**
in vivo Circumferential Stretch (λ_ϑ)	1.77 +/- 0.03	1.81 +/- 0.02	1.48 +/- 0.03**	1.94 +/- 0.05	1.80 +/- 0.04	1.72 +/- 0.02*
in vivo Axial Stretch (λ_z^{iv})	1.80 +/- 0.05	1.75 +/- 0.03	1.48 +/- 0.03**	1.50 +/- 0.03	1.60 +/- 0.05	1.50 +/- 0.02
Systolic Cauchy Stresses (kPa)						
Circumferential, σ_ϑ	486 +/- 26.5	424 +/- 21.1	130 +/- 8.5**	335 +/- 16.1	313 +/- 17.2	138 +/- 4.8**
Axial, σ_z	500 +/- 46.3	412 +/- 12.3	114 +/- 4.6**	306 +/- 8.1	296 +/- 14.3	156 +/- 11.2**
Systolic Linearized Stiffness (MPa)						
Circumferential, $\mathbb{C}_{\theta\theta\theta\theta}$	2.59 +/- 0.17	2.71 +/- 0.07	2.48 +/- 0.25	2.12 +/- 0.17	2.16 +/- 0.18	1.76 +/- 0.14
Axial, $\mathbb{C}_{zzzz}$	2.58 +/- 0.28	2.50 +/- 0.13	1.83 +/- 0.13*	4.14 +/- 0.24	4.49 +/- 0.24	3.82 +/- 0.30
Distensibility (1/MPa)	23.03 +/- 1.22*	18.73 +/- 0.91	3.92 +/- 0.21**	20.57 +/- 1.91	17.89 +/- 1.82	8.04 +/- 0.44**
Systolic Stored Energy (kPa)	156 +/- 13.8*	124 +/- 6.1	18 +/- 1.2**	89 +/- 4.4	81 +/- 5.3	24 +/- 0.8**

Mean ± SEM values of all geometric and mechanical metrics calculated from the ex vivo biomechanical testing, including unloaded dimensions and values representing in vivo conditions at group specific systolic pressures and axial stretches for both the ascending thoracic aorta (ATA) and proximal thoracic aorta (DTA). *P < 0.05 vs. hBAC-mWT and WT, **P < 0.001 vs. hBAC-mWT and WT; one-way ANOVA. See Fig. 3 in the main paper for graphical representation of many of these values.

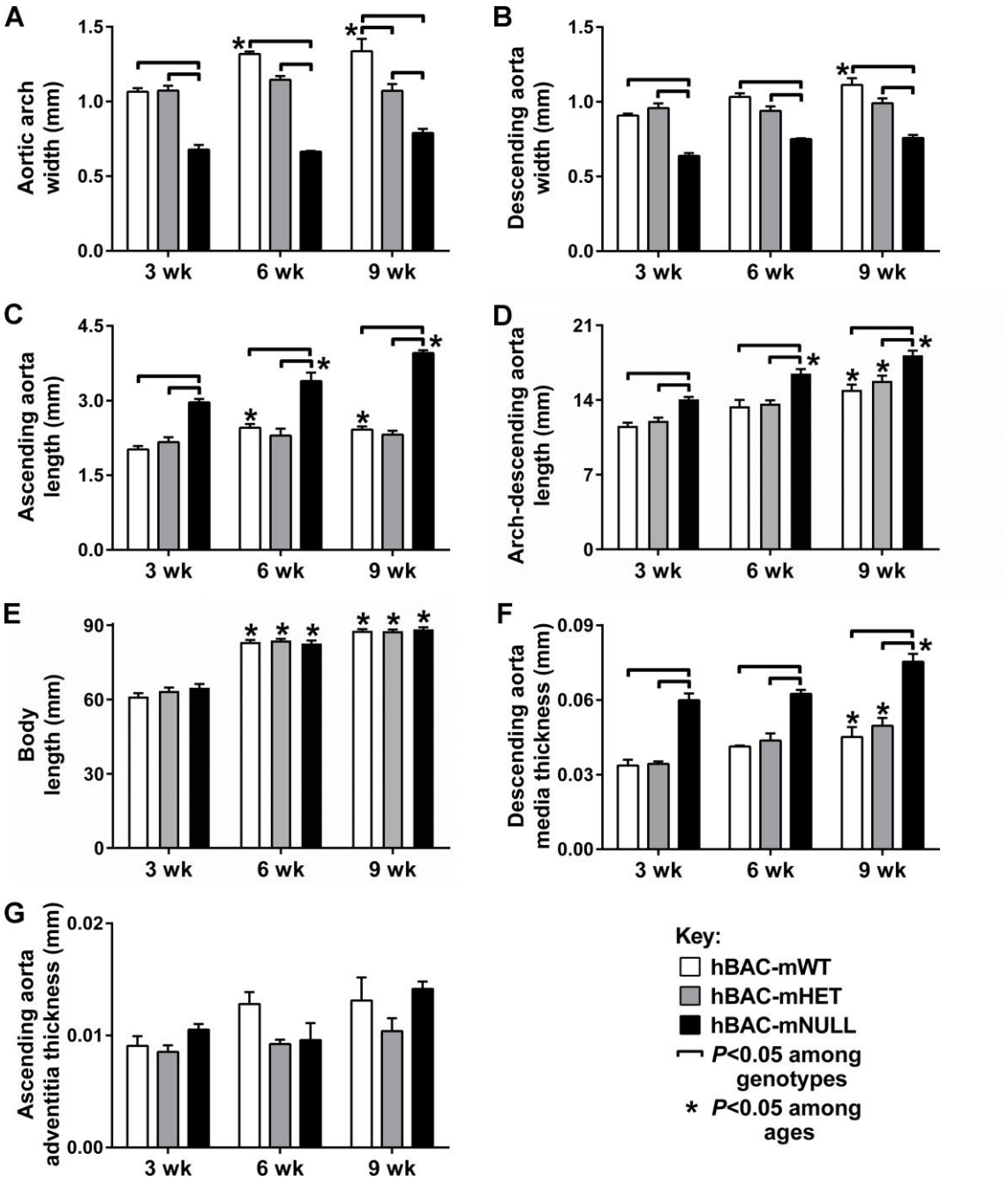

Figure I: Aortic Dimensions in Elastin-Deficient Mice. Thoracic aortas of hBAC-mWT (white bars), hBAC-mHET (gray bars), and hBAC-mNULL (black bars) mice were analyzed at 3, 6, and 9 weeks of age. In situ width (i.e., external diameter) of (***A***) aortic arch and (***B***) descending aorta. In situ length of (***C***) ascending aorta, (***D***) arch and descending aorta, and (***E***) body. Thickness of (***F***) media of descending aorta and (***G***) adventitia of ascending aorta. Data represent mean ± SEM; n = 3 (6 weeks) to 6 (3 and 9 weeks); ¯$P < 0.05$ among genotypes and *$P < 0.05$ among ages; two-way ANOVA.

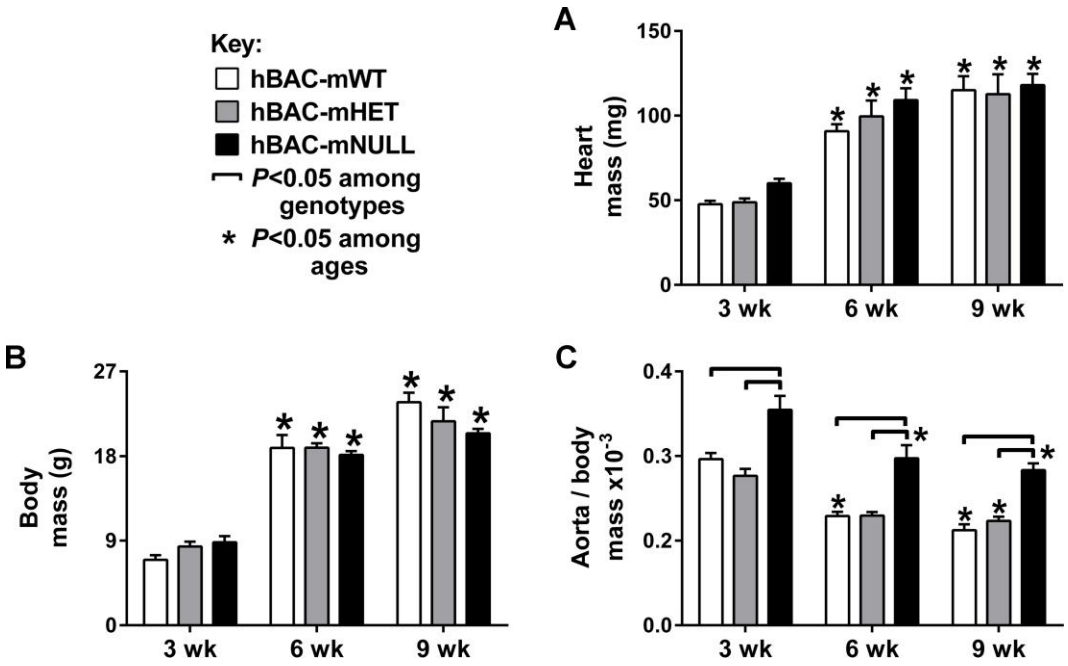

Figure II: Organ and Body Mass in Elastin-Deficient Mice. hBAC-mWT (white bars), hBAC-mHET (gray bars), and hBAC-mNULL (black bars) mice were analyzed at 3, 6, and 9 weeks of age. (***A***) Heart mass, (***B***) body mass, and (***C***) an index of thoracic aorta mass to body mass were determined. Data represent mean ± SEM; n = 3 (6 weeks) to 6 (3 and 9 weeks); ¯$P < 0.05$ among genotypes and *$P < 0.05$ among ages; two-way ANOVA.

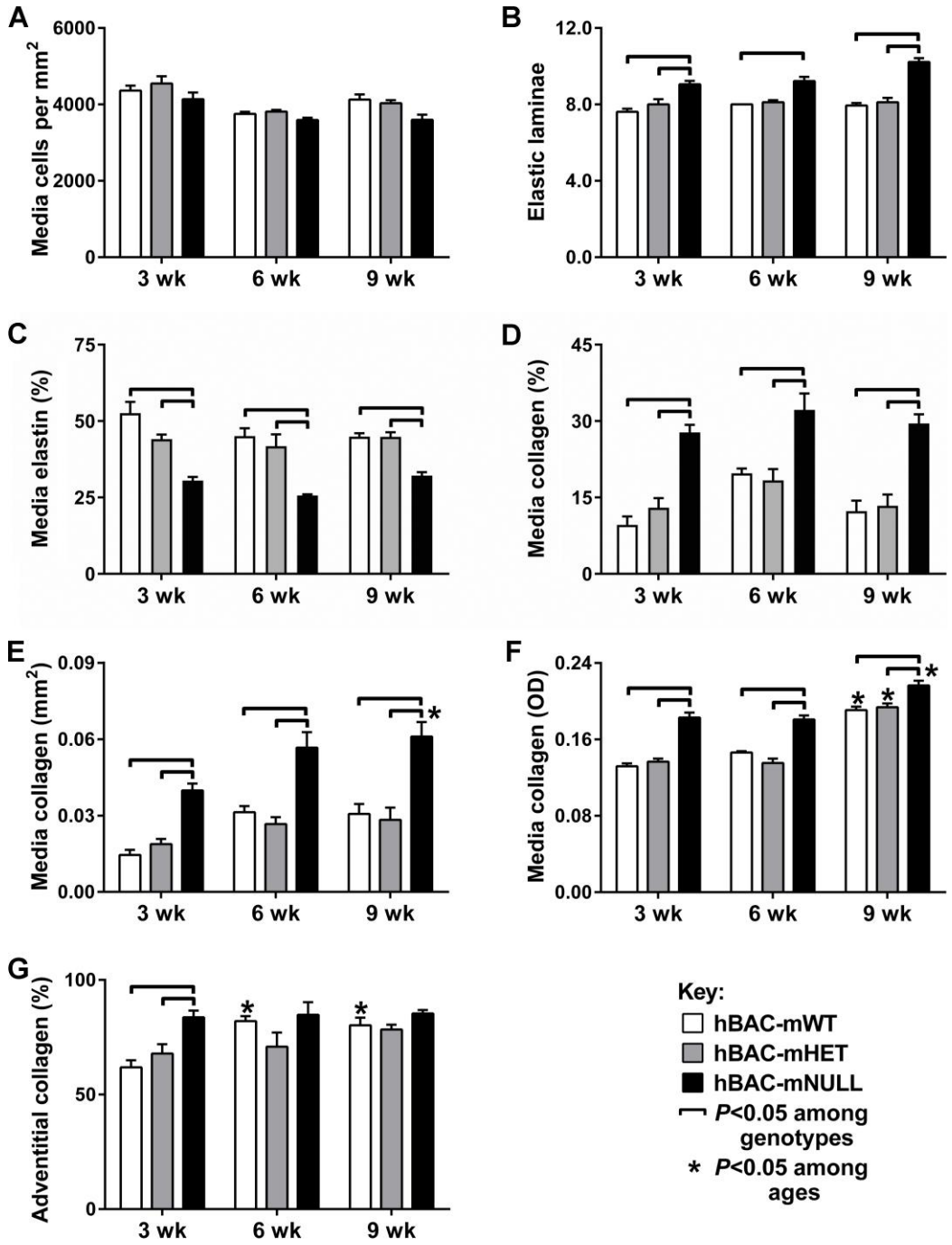

Figure III: Structure of Elastin-Deficient Aortas. Thoracic aortas of hBAC-mWT (white bars), hBAC-mHET (gray bars), and hBAC-mNULL (black bars) mice were analyzed at 3, 6, and 9 weeks of age. (***A***) Number of medial cells per cross-sectional area in ascending aortas. (***B***) Number of elastic laminae in ascending aortas. (***C***) Percent of media staining positive for elastin in descending aortas. (***D***) Percent of media staining positive with sirius red in descending aortas. (***E***) Medial area staining positive with sirius red in ascending aortas. (***F***) Intensity of sirius red staining in media of ascending aortas. (***G***) Percent of adventitia staining positive with sirius red in ascending aortas. Data represent mean ± SEM; n = 3 (6 weeks) to 6 (3 and 9 weeks); ¬ $P < 0.05$ among genotypes and * $P < 0.05$ among ages; two-way ANOVA.

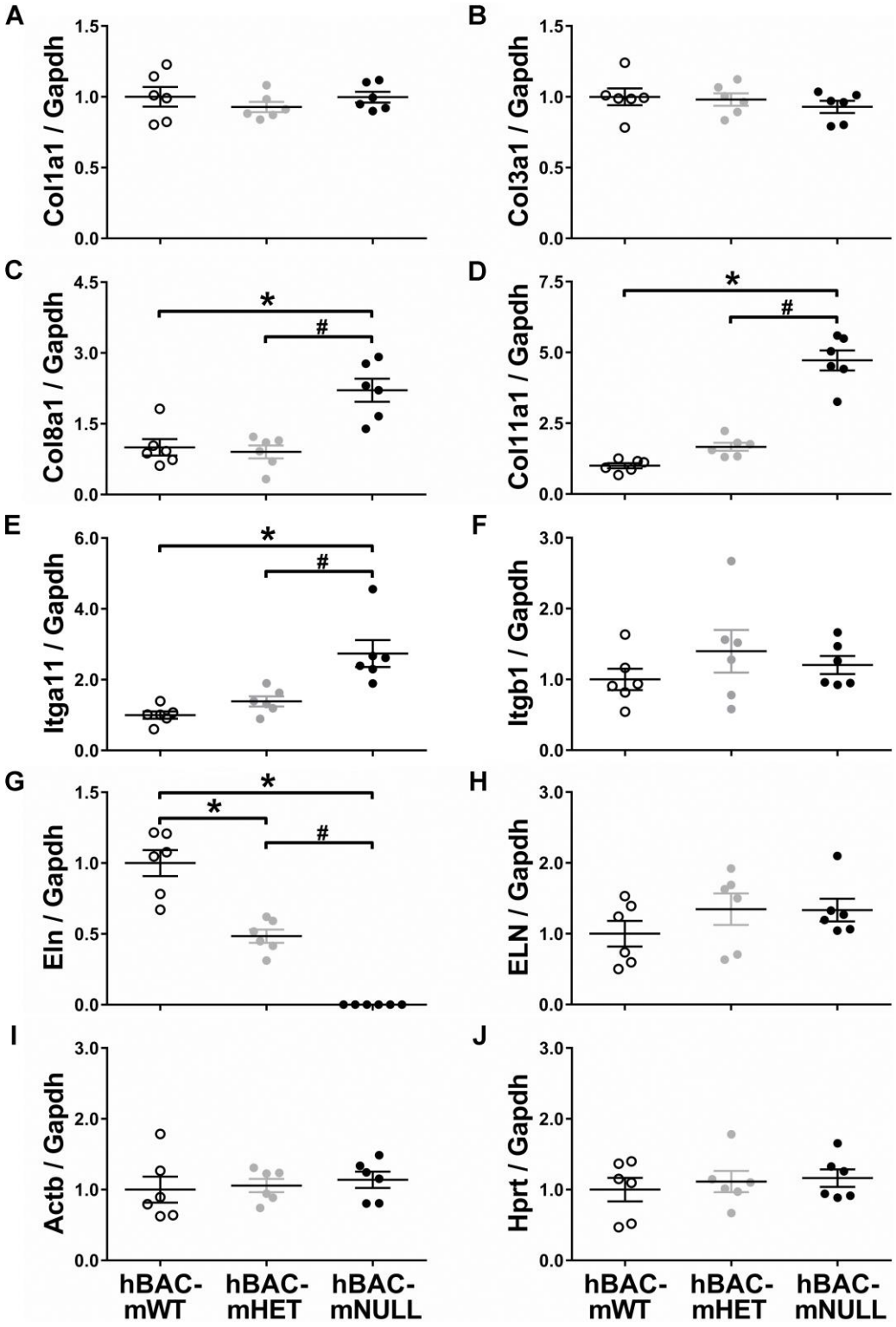

Figure IV: Expression of Collagen and Related Molecules. RNA was isolated from thoracic aortas of hBAC-mWT (white symbols), hBAC-mHET (gray symbols), and hBAC-mNULL (black symbols) mice at 3 weeks of age and analyzed by qRT-PCR. Transcripts for (***A***) *Col1a1*, (***B***) *Col3a1*, (***C***) *Col8a1*, (***D***) *Col11a1*, (***E***) *Itga11*, (***F***) *Itgb1*, (***G***) *Eln*, (***H***) *ELN*, (***I***) *Actb*, and (***J***) *Hprt*, relative to *Gapdh* were normalized to the mean of controls (i.e., hBAC-mWT). Data represent mean ± SEM; $n = 6$; $^{*}P < 0.05$ vs. hBAC-mWT and $^{\#}P < 0.05$ vs. hBAC-mHET; one-way ANOVA.

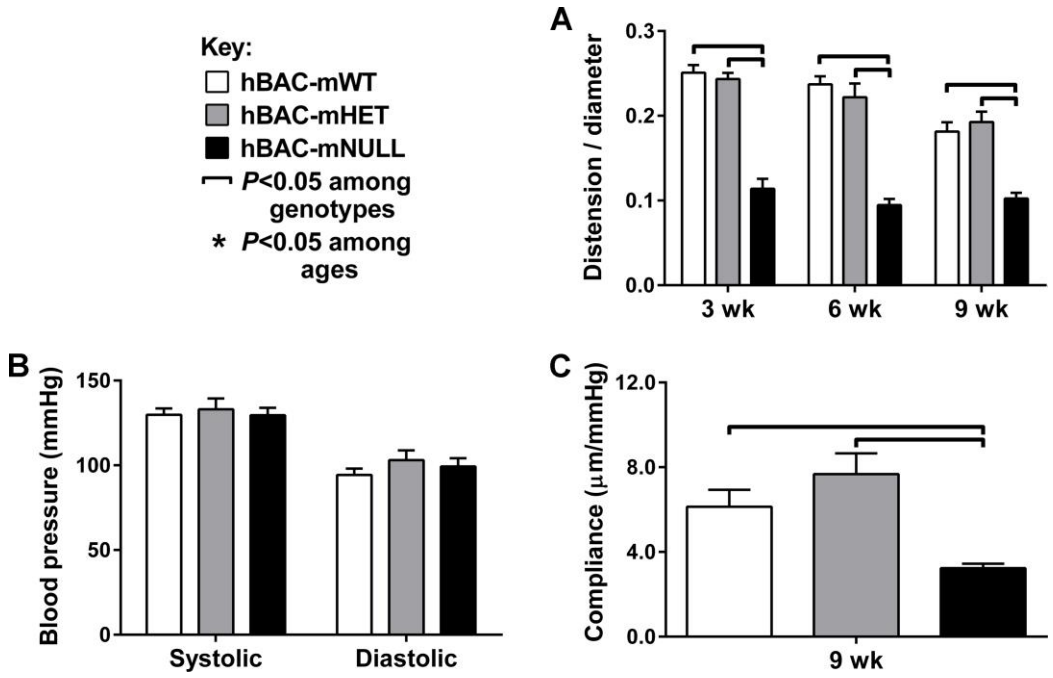

Figure V: Function of Elastin-Deficient Aortas. Ascending aorta of hBAC-mWT (white bars), hBAC-mHET (gray bars), and hBAC-mNULL (black bars) mice were imaged by ultrasound in vivo at 3, 6, and 9 weeks of age and blood pressure was determined by tail-cuff at 9 weeks of age. (***A***) Aortic distension (change in diameter) indexed to end-diastolic aortic diameter. (***B***) Systolic and diastolic blood pressure. (***C***) Aortic compliance defined as change in diameter per change in blood pressure. Data represent mean ± SEM; n = 3 (6 weeks) to 6 (3 and 9 weeks); ¯$P < 0.05$ among genotypes; one-way ANOVA.

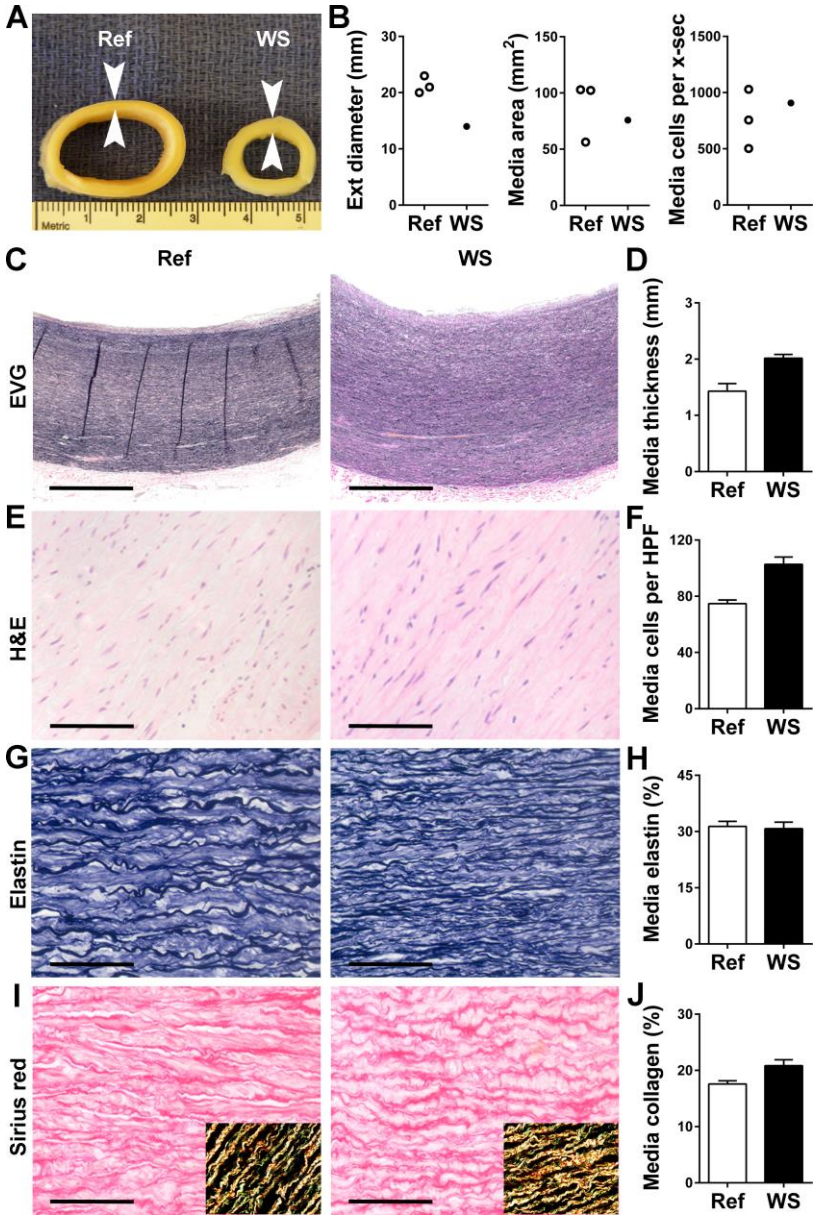

Figure VI: Analysis of Human Proximal Descending Aortas. (***A***) Descending aorta ring from WS subject compared with that of age- and sex-matched referent (ref) subject; arrows delineate vessel wall thickness. (***B***) Measurements of external (ext) diameter, medial area, and total number of medial cells per cross-section (x-sec) in WS specimen and 3 referent descending aortas. (***C***) Representative images of EVG-stained cross-sections (bars: 1 mm). (***D***) Medial thickness measured at 4 separate points. (***E***) Representative images of H&E stain (bars: 100 µm). (***F***) Medial cell density determined in 9 high power fields (HPF). (***G***) Representative images of elastin stain (bars: 100 µm). (***H***) percent of media staining positive for elastin in 9 high power fields. (***I***) Representative images of sirius red stain (bars: 100 µm) with polarized light images in insets confirming collagen detection. (***J***) Percent of media staining positive for collagen in 9 high power fields. Data represent mean ± SEM; *n* = 4-9 replicates from 1 WS specimen vs. 3 referent descending aortas.

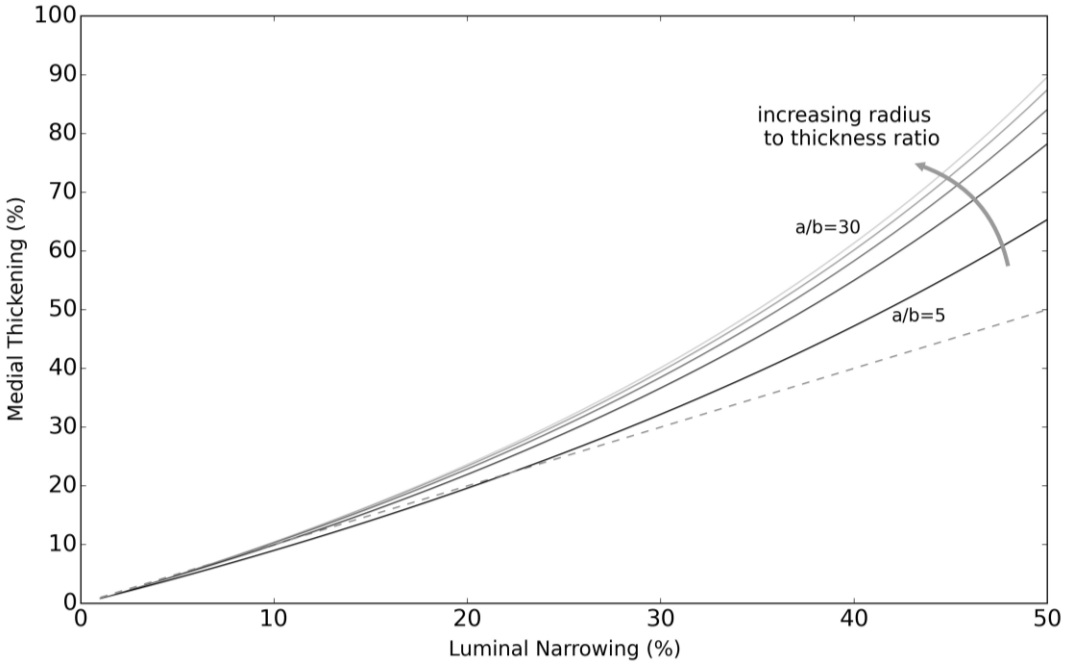

Figure VII: Relationship Between Medial Thickness and Luminal Radius During Medial Remodeling with Area Conservation. Using Equation (1) of Appendix I above, we plot the percent *increase* in medial thickness (y-axis: $(\beta - 1) \cdot 100$) that is needed for each percent *decrease* in luminal radius (x-axis: $(1 - \alpha) \cdot 100$) for various possible values of the normal ratio of radius:thickness (a/b) from 5 to 30. For purposes of comparison, the line of identity (i.e., if percent changes were equal) is shown as a straight dashed line. Note, therefore, that conservation of medial area increasingly requires greater thickening as the lumen narrows.